ELSEVIER

Deep-Sea Research II 52 (2005) 1325–1343

DEEP-SEA RESEARCH
PART II

www.elsevier.com/locate/dsr2

Multiscaling statistical procedures for the exploration of biophysical couplings in intermittent turbulence. Part II. Applications

Laurent Seuront[a,b,*], François G. Schmitt[a]

[a]*Ecosystem Complexity Research Group, Station Marine de Wimereux, CNRS UMR 8013 ELICO, Université des Sciences et Technologies de Lille, 28 avenue Foch, BP 80, F-62930 Wimereux, France*
[b]*School of Biological Sciences, Flinders University, GPO Box 2100, Adelaide 5001, Australia*

Accepted 18 January 2005

Abstract

Turbulence has widely been recognized as a source of homogeneity in phytoplankton distributions at scales of less than 1 m. However, it is shown here, using univariate and bivariate procedures specifically developed to investigate the properties of single and joint intermittent stochastic processes, that the small-scale phytoplankton distribution investigated in the Eastern English Channel over four tidal cycles is never fully homogenized and presents a differential coupling with temperature, for turbulent intensities ranging from 5×10^{-7} to $10^{-4}\,m^2\,s^{-3}$. More specifically, patchiness increases with decreasing turbulence intensity, and is higher during ebb than during flood tide for similar turbulence intensities. The coupling between phytoplankton and temperature distributions increases with increasing turbulence intensity, and is stronger during flood tide. Taking into account the hydrodynamic and tidal characteristics of the study area, as well as the composition of the phytoplankton community, phenomenological explanations are provided for the observed patterns converging towards a combination of biologically and physically induced patchiness, and turbulence-controlled biophysical couplings. Taking into account the detailed intermittent complexity of marine data sets can lead to a valuable, unique gain in understanding structures and functions of marine ecosystems.

1. Introduction

Moving beyond the long-standing assumption that turbulence homogenizes phytoplankton distributions at scales of less than 1 m, the existence of patchiness in phytoplankton distributions, measured at scales of centimetres to tens of centimetres, has been widely reported (Cassie, 1963; McAlice, 1970; Mitchell and Fuhrman, 1989; Owen, 1989; Cowles et al., 1993; Waters and Mitchell, 2002; Waters et al., 2003), suggesting that microscale phytoplankton patchiness is a ubiquitous feature of the marine environment.

*Corresponding author. Fax: +33 3 21992901.
E-mail address: laurent.seuront@univ-lille1.fr (L. Seuront).

0967-0645/$ - see front matter © 2005 Elsevier Ltd. All rights reserved.
doi:10.1016/j.dsr2.2005.01.005

This indicates that further investigation is needed to elucidate the structure of phytoplankton distributions at small-scales, where the most ecologically relevant processes of viral infection (Furhman, 1999), nutrient uptake (Karp-Boss et al., 1996; Blackburn et al., 1998), aggregate formation (Kiørboe, 2001), light harvesting (Kirk, 1994), predator–prey interactions (Gerritsen and Strickler, 1977) and behavior (Kamykowski et al., 1997; Seuront et al., 2005) occur. In particular, the potential effects of turbulence on small-scale phytoplankton patchiness is a crucial process to investigate. Periodic advections of water masses of different physical and biological properties are ubiquitous in tidally driven coastal ecosystems (Tomczak and Godfrey, 1994; Mann and Lazier, 1996), and can have salient effects on the structure and function of estuarine, coastal and intertidal environments (Yin and Harrison, 2000; Smayda, 2002). Nevertheless, little attention has been paid previously to the potential differential effects of these processes on small-scale phytoplankton patchiness. The first-order question is thus to know when phytoplankton cells' small-scale intermittent distributions mostly reflect physical forcing and when they can be regarded as being independent of their surrounding physical environment? Indeed, the clear effects of microscale turbulence on pelagic ecosystems (Marrasé et al., 1997; Peters and Marrasé, 2000), together with the evidence that turbulent processes can generate microscale patchiness rather than randomness in phytoplankton (Jaffe et al., 1998; Seuront et al., 1996a, b, 1999), suggest that turbulence could control phytoplankton small-scale distributions. On the other hand, the extreme similarity observed between small-scale intermittent distributions of temperature, salinity and phytoplankton biomass (Seuront et al., 1999) suggests a passive behavior of phytoplankton cells in the turbulent flows.

Our high-frequency (2 Hz) fluorescence and temperature time series were recorded in a highly dissipative tidally mixed coastal ecosystem, the Eastern English Channel, under significantly fluctuating tidal and turbulent conditions. The aim of this study is thus to demonstrate when (i) small-scale phytoplankton patchiness and (ii) the couplings between phytoplankton and a purely passive scalar (e.g., temperature) are controlled by turbulence intensity and tidal advective processes. It is stressed here that because of the dissipative nature of the investigated water column, this study specifically relates to horizontal patchiness in an unstratified water column, and is therefore not relevant for the vertical phytoplankton variability that forms in a stratified water column, and might result from buoyancy effects, vertical gradients of nutrients and/or the exponential light profile. The results, indicating that phytoplankton patchiness increases with decreasing turbulence intensity and is always higher during ebb tide for a given turbulence intensity, are used to infer the relative dominance between potential physical and biological structuring mechanisms operating at small scales.

2. Methods

2.1. Field site and sampling strategy

Sampling was conducted from 28 to 30 March 1998, at an anchor station (Fig. 1) located in the offshore waters of the Eastern English Channel (50°40′75N, 1°24′60E) for 54 h (~4.5 tidal cycles) during the spring tide. The tidal range, bounded between 3 and 9 m, in this area is one of the largest

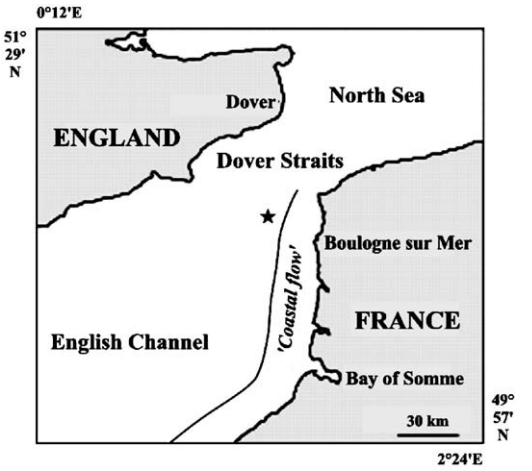

Fig. 1. Study area and location of the sampling station (★) in the Eastern English Channel.

in the world, and tides are characterized by a residual circulation parallel to the coast, with nearshore coastal waters drifting from the English Channel into the North Sea. Coastal waters, also referred to as a 'coastal flow' (Brylinski et al., 1991), are influenced by freshwater run-off from the Seine Estuary to the Straits of Dover, and separated from offshore waters by a transient, tidally controlled frontal area (Brylinski and Lagadeuc, 1990; Lagadeuc et al., 1997). The region is characterized by its low salinity, turbidity (Dupont et al., 1991), phytoplankton richness (Brylinski et al., 1984) and productivity (Brunet et al., 1992, 1993). More specifically, the sampling location was chosen because the physical and hydrological properties are representative of the coastal water flow encountered in the Eastern English Channel (Brunet et al., 1992; Seuront et al., 1999, 2002).

High-resolution time series were collected at 2 Hz, simultaneously from a single depth (10 m) for temperature, regarded as a passive scalar under physical control, together with in vivo fluorescence, a proxy of phytoplankton biomass, with a Sea-Bird Sealogger CTD probe and a SeaTech fluorometer, respectively. Measurements of physical parameters (temperature and salinity) and in vivo fluorescence were taken every hour from the surface to the bottom with a Sea-Bird 19 Sealogger CTD and a SeaTech fluorometer. Current speed and direction were measured every 5 min at 3, 6 and 10 m with Anderra current meters. Wind data were collected every hour with the on-board anemometer. Calibration water samples were taken every hour from a depth of 10 m using Niskin bottles, and chlorophyll *a* concentrations were estimated following Strickland and Parsons (1972) from 1-l filtered frozen samples, extracted with 90% acetone, and assayed in a spectrophotometer.

2.2. Quantifying turbulent kinetic energy dissipation rates

In the Eastern English Channel, the turbulent kinetic energy is mainly generated by tidal processes (Seuront et al., 1999, 2002). The dissipation rate of turbulent energy induced by the tidal flow ε_t ($m^2 s^{-3}$) was estimated following MacKenzie and Leggett (1993):

$$\varepsilon_t = \phi u^3/h, \tag{1}$$

where ϕ, u and h are the fraction of the tidal energy used for vertical mixing ($\phi = 0.006$, Bowers and Simpson, 1987), the M_2 depth-averaged velocity of the tidal flow ($m s^{-1}$) and the depth of the water column (m), respectively. Values of ε_t exceeding $2.4 \times 10^{-5} m^2 s^{-3}$ are typical of tidally mixed waters (MacKenzie and Leggett, 1991).

The vertical stability of the water column cannot be estimated by the Richardson number (*Ri*) nor static stability (N^2) because the water column always has no vertical structure, i.e. essentially no vertical gradient of density at the scale of resolution. Nevertheless the dynamic stability of the water column was estimated using the total shear squares (Itsweire et al., 1989):

$$S^2 = (\Delta u/\Delta z)^2 + (\Delta v/\Delta z)^2, \tag{2}$$

where Δz is variation in depth, and Δu and Δv are variations in the instantaneous speed of the 2 orthogonal components u (cross-channel) and v (along-channel) of the tidal current, respectively.

2.3. Quantifying phytoplankton patchiness

2.3.1. Investigating scaling properties: spectral analysis

Spectral analysis has been widely used in ecology to separate and measure the amount of variability (i.e. the variance) occurring in different wavenumber bands. In particular, assuming local isotropy and three-dimensional homogeneity of turbulence in the inertial subrange, the fluctuations of a given scalar quantity passively advected by turbulence (i.e. temperature, and fluorescence, a priori phytoplankton cells) can be described in Fourier space by the spectral densities $E_T(f)$ and $E_F(f)$ following:

$$E_T(f) \approx f^{-\beta_T},$$

$$E_F(f) \approx f^{-\beta_F}, \tag{3}$$

where f is a frequency, and $\beta_T = \beta_F = \frac{5}{3}$ for a non-intermittent turbulence (Kolmogorov, 1941; Obukhov, 1941, 1949; Corrsin, 1951). Power spectra

have been obtained performing fast Fourier transform (FFT, Press et al., 1992) on detrended (i.e. stationary) time series.

2.3.2. Investigating multiscaling properties: structure functions

Fully developed turbulence is now known to be an extremely intermittent process (for reviews see Frisch, 1995; Jiménez, 1997; Jou, 1997; Seuront and Schmitt, 2005). Turbulent kinetic energy and scalar distributions of temperature and salinity exhibit strong gradients that are the largest at scales similar to the Kolmogorov microscale, i.e. the viscous scale where viscosity effects cannot be neglected and start to smooth out turbulent fluctuations (Gargett, 1997; Sanford, 1997). These intermittent fluctuations have been analyzed in the multifractal framework (Pascual et al., 1995; Seuront et al., 1996a, b, 1999, 2002; Lovejoy et al., 2001), with statistical tools devoted to characterize intermittent fields. Thus, whereas random variability often has been modelled in marine ecology in the Gaussian framework, though, e.g., Gaussian distributions and Brownian motion (Yamazaki and Okubo, 1995; Visser, 1997), we will here generalize this approach and fully take into account the intermittency of in situ temperature and fluorescence temporal distributions. We will only review the main properties of multiscaling patterns and processes. More details on the use of related algorithms to marine ecology studies, and on what can be concluded from their use, can be found in Seuront et al. (1999).

Under fairly general conditions, the properties of the probability distribution of a random variable are equivalently specified by its statistical moments. The latter corresponds to the introduction of the qth order structure functions defined as:

$$\langle(\Delta T(\tau))^q\rangle = \langle|T(t+\tau) - T(t)|^q\rangle$$

$$\langle(\Delta F(\tau))^q\rangle = \langle|F(t+\tau) - F(t)|^q\rangle \quad (4)$$

where $\langle\cdot\rangle$ indicates statistical averaging and $\langle(\Delta T(\tau))^q\rangle$ and $\langle\Delta F(\tau))^q\rangle$ are the qth order statistical moments of the fluctuations of temperature and fluorescence at scale τ, respectively. The scale-invariant structure function exponents $\zeta_T(q)$ and $\zeta_F(q)$ then describe the multiscaling of the statistical moments of order q of the temperature and fluorescence fields as

$$\langle(\Delta T_\tau)^q\rangle \approx \tau^{\zeta_T(q)},$$

$$\langle(\Delta F_\tau)^q\rangle \approx \tau^{\zeta_F(q)}, \quad (5)$$

where τ is the time scale and the angle brackets "$\langle\cdot\rangle$" indicate statistical averaging. The scaling exponents $\zeta_T(q)$ and $\zeta_F(q)$ are, respectively, estimated by the slope of the power-law trends of $\langle(\Delta T_\tau)^q\rangle$ and $\langle(\Delta F_\tau)^q\rangle$ vs. τ, giving linear curves in a log–log plot. For monoscaling processes, the function $\zeta(q)$ is linear: $\zeta(q) = qH$ [$\zeta(q) = q/2$ for Brownian motion and $\zeta(q) = q/3$ for the Kolmogorov-Obukhov (1941) picture of non-intermittent turbulence]. For multiscaling processes, this function is non-linear and concave.

Finally, we should note here that in the multiscaling framework, intermittency is taken into account as:

$$\beta_T = 1 + \zeta_T(2),$$

$$\beta_F = 1 + \zeta_F(2). \quad (6)$$

We can thus see that the intermittency corrections introduced by the second term of Eq. (6) lead to $\beta_T > \frac{5}{3}$ and $\beta_F > \frac{5}{3}$ (e.g. Seuront and Schmitt, 2005; Seuront et al., 2005).

2.4. Quantifying biophysical couplings

2.4.1. Scaling test for independence: coherency analysis

The squared-coherence between temperature and fluorescence time series is estimated from cross-spectrum $E_{TF}(f)$, and power spectrum $E_A(f)$ and $E_B(f)$ as (Legendre and Legendre, 1998):

$$K^2_{TF}(f) = \frac{E^2_{TF}(f)}{E_T(f)E_F(f)}, \quad (7)$$

where the cross-spectrum $E_{TF}(f)$ is formed by FFT of the cross-correlation function between temperature and fluorescence time series. While power spectra $E_T(f)$ and $E_F(f)$ are directly related to the autocorrelation, Eq. (7) leads to consider the squared-coherence $K^2_{TF}(f)$ between two time series as an analogue for a given frequency f of the squared cross-correlation coefficient r^2_{TF} between

two time series formed from the variance and covariance estimates [$v_{ii}(l)$ and $v_{ij}(l)$, respectively], all taken at zero spatial lag as:

$$r_{TF}^2(0) = \frac{v_{TF}^2(0)}{v_{TT}(0)v_{FF}(0)}. \quad (8)$$

Finally, we plot $K_{TF}^2(f)$ for different values of the frequency f, thereby obtaining an estimate of the spatial rate at which vertical patterns of two different time series evolve and decorrelate.

2.4.2. Multiscaling test for independence: "Generalized Correlation Functions" (GCF)

Instead of random variables X and Y leading to the standard correlation coefficient defined in Eq. (9), in the multiscaling framework we consider here the two stochastic processes (ΔT_τ) and (ΔF_τ) characterized by their pth and qth order structure functions as $\langle(\Delta T_\tau)^p\rangle \approx \tau^{\zeta_T(p)}$ and $\langle(\Delta F_\tau)^q\rangle \approx \tau^{\zeta_F(q)}$ [cf. Eq. (5)]. The correlation between the two processes $(\Delta T_\tau)^p$ and $(\Delta F_\tau)^q$ then becomes a function of the scale and of the statistical orders of moment p and q, expressed by the "Generalized Correlation Functions" (GCF hereafter) $c(p,q)$ as (Seuront and Schmitt, 2005):

$$c(p,q) = \frac{\langle[(\Delta T_\tau)^p(\Delta F_\tau)^q]\rangle}{\langle(\Delta T_\tau)^p\rangle\langle(\Delta F_\tau)^q\rangle} \approx \tau^{-r(p,q)}, \quad (9)$$

where for more generality we take $p \neq q$, and $r(p,q) \geqslant 0$; see Seuront and Schmitt (2005) for further details. One may note here that at a given scale τ, if the fluctuations of the stochastic processes (ΔT_τ) and (ΔF_τ) are independent, we have $c(p,q) = 0$, for any combination of p and q. Increasing values of $c(p,q)$ would thus characterize increasing dependence between $(\Delta T_\tau)^p$ and $(\Delta F_\tau)^q$. The "Generalized Correlation Exponents" (GCE hereafter) $r(p,q)$ are estimated as the slopes of the power-law trends of $c(p,q)$ vs. τ in a log–log plot. It can be easily seen that in the particular case where $p = q = 1$, Eq. (10) leads to the basic expression of the correlation coefficient between (ΔT_τ) and (ΔF_τ). The GCF can thus be thought as a way to describe the evolution of the correlation between two stochastic processes $(\Delta T_\tau)^p$ and $(\Delta F_\tau)^q$ with scale. In the GCF/GCE framework, if the fluctuations of the stochastic processes (ΔT_τ) and (ΔF_τ) are independent, we thus have:

$$r(p,q) = 0 \quad (10)$$

for any combination of p and q. In contrast, and more generally speaking, the more $r(p,q)$ is positive, the more $(\Delta T_\tau)^p$ and $(\Delta F_\tau)^q$ are dependent random variables.

The main advantages of this technique are that (i) it makes no assumptions about the spectrum nor the probability distribution of either data sets, (ii) it takes into account the multiscale intrinsic properties of intermittent processes, (iii) it allows to test for the phenomenology responsible for the high-intensity (rare and unexpected) fluctuations observed in intermittent distributions considering their potential association with both high- and low-intensity fluctuations characterized by high and low orders of moment, respectively, as we shall see with the data analysis presented below. The Generalized Correlation Functions and Exponents thus provide a general framework as they express the correlation between the fields (ΔT_τ) and (ΔF_τ), together with their scale dependence and their moment dependence. This indicates if high-intensity fluctuations of one field are highly correlated to low intensities of the other (or in other words if the gradients of two fields are proportional or inversely proportional), and the scales over which these correlation occurs.

3. Ocean passive and "biologically active" scalars

3.1. Hydrodynamic conditions and phytoplankton biomass

At all depths, current vectors showed wide variations, related to the semidiurnal M_2 (12.4 h) tidal component. This resulted in variations of ~6 h periodicity in the current speed, which ranged from 3 to 132 cm s^{-1}, 4 and 128 cm s^{-1} and 3 and 129 cm s^{-1} at respectively 3, 6 and 9 m depth. No significant differences were detected between mean current speed and direction at all three depths investigated (Kruskal–Wallis test, $p < 0.01$). The related depth-averaged mean dissipation rates, $\varepsilon_T = 7.14 \times 10^{-5}$ m^2 s^{-3}, ranged from 1.55×10^{-7} to 4.11×10^{-4} m^2 s^{-3}, which is characteristic of a

strongly mixed tidal area. The vertical shear activity, S^2 ($S^2 = 9.25 \times 10^{-3}\,s^{-2}$), which can generate turbulence, was always higher than $2.4 \times 10^{-4}\,s^{-2}$, a low shear effect according to Itsweire et al. (1989), indicating an elevated turbulence in the water column. Temperature exhibited a significantly autocorrelated 12 h tidal cycle, with a superimposed diel cycle (sinusoidal regression, $r^2 = 0.68$).

The chlorophyll-*a* concentration was $12.35 \pm 4.25\,\mu g\,l^{-1}$ ($\bar{x} \pm SD$). No decrease in fluorescence was observed in the surface layers or at the sampling depth during the daylight period, indicating the absence of photoinhibition (Falkowski and Kiefer, 1985). In addition, as chlorophyll-*a* concentrations appear significantly correlated with fluorescence (Kendall's $\tau = 0.675$, $p < 0.01$), the high-frequency fluorescence data recorded in the present study can then be regarded as a direct and reliable estimate of chlorophyll-*a*. Autocorrelation analysis of chlorophyll-*a* identified a significant ($p < 0.05$) 12-h tidal cycle in chlorophyll-*a* concentrations. In addition, cross-correlation analysis between current direction and chlorophyll-*a* showed that chlorophyll-*a* was positively correlated ($p < 0.05$) with tidal current direction. This is related to the tidally driven advective processes occurring in the Eastern English Channel between inshore and offshore waters. During flood tide, the phytoplankton depleted offshore waters are advected towards the coast, leading to a decrease in fluorescence. Conversely during ebb tide, the phytoplankton rich inshore waters are advected offshore, leading to an increase in fluorescence. One must also note here that the specific composition of phytoplankton assemblages is also likely to differ between inshore and offshore waters (Martin-Jezequel, 1983; Brylinski et al., 1984).

3.2. Turbulence and phytoplankton patchiness

Considering the role played by turbulence in the formation and disruption of particle aggregates (e.g., Kiørboe, 2001, and references therein) and the highly varying dissipation rates of turbulent energy observed over a tidal cycle in this area (between 10^{-6} and $10^{-4}\,m^2\,s^{-3}$; Seuront et al., 2002), the question addressed here is whether the local hydrodynamic conditions have an effect on both temperature and phytoplankton biomass local distributions. To avoid potential spurious results stemming from any 'population-dependent' and 'density-dependent' effects related to the advective processes highlighted above, subsets of in vivo fluorescence of comparable intensity (within one standard deviation of the whole time series) that have been analyzed separately in the framework of flood and ebb tides have been selected. From the original time series recorded at 2 Hz (i.e. 193,918 data), we then built six sets of four fluorescence subseries of one hour (i.e. 3600 data), each set corresponding to a different level of dissipation rates ranging from $\varepsilon = 5 \times 10^{-7}$ to $10^{-4}\,m^2\,s^{-3}$ in flood and ebb tide conditions. Twenty-four 1-h duration time series of in vivo fluorescence in both flood and ebb tide conditions were thus analyzed. For the sake of comparison, and to provide a reference framework that can be related to purely passive scalars, the original temperature time series also has been subsampled. The related dissipation rates ε_t are similar, respectively ranging from 5.01×10^{-7} to $1.56 \times 10^{-4}\,m^2\,s^{-3}$ and from 5.51×10^{-7} to $3.73 \times 10^{-4}\,m^2\,s^{-3}$ in ebb and flood tide. Analysis of these data subsets thus allows direct comparisons of the effect of turbulence on patchiness of inshore and offshore phytoplankton populations. We subsequently conducted both spectral and multifractal analyses on each subseries of temperature and fluorescence within a given subset.

The double logarithmic power spectra for temperature and fluorescence time series are given in Fig. 2. Log–log linearity of power spectra is very strong for the whole range of available scales considered, with coefficient of determination (r^2) ranging from 0.97 to 0.99. The slopes β_T and β_F, estimated for the frequency bands that maximized the coefficient of determination and minimized the total sum of squared-residuals for the regression in log–log plots of the temperature and fluorescence power spectra, cannot be statistically distinguished within each set of temperature and fluorescence subseries (analyses of covariance, $p > 0.05$), nor between the six sets considered ($p > 0.05$). These results, fully congruent with previous studies conducted in the same area (Seuront et al.,

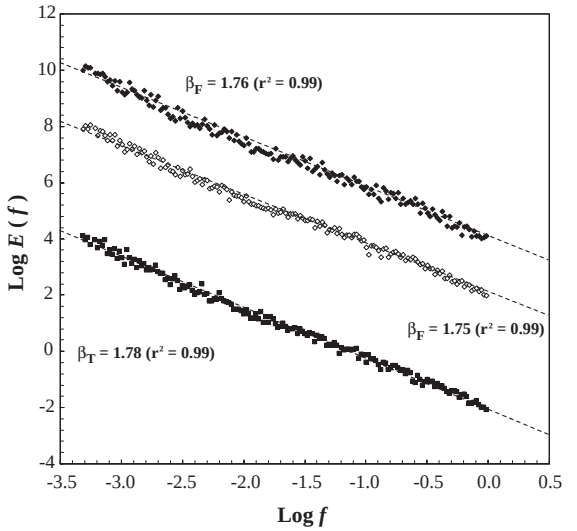

Fig. 2. Log–log plots of the power spectra $E(f)$ of temperature (black squares), and in vivo fluorescence (diamonds) recorded during flood tide (open diamonds) and ebb tide (black diamonds). The dashed lines are the best linear regressions found for each parameter and indicate their scaling range.

1996a, b, 1999, 2002), suggest an extreme similarity between the single scaling properties of small-scale temperature and fluorescence distributions. At this stage, fluorescence can then still be regarded as being a passive scalar.

The qth order structure functions confirm the scaling previously shown by spectral analysis. The temperature and fluorescence structure functions, $\langle(\Delta T(\tau))^q\rangle$ and $\langle(\Delta F(\tau))^q\rangle$, exhibit a clear linear behavior as a function of scale in a log–log plot for different orders of moment (Fig. 3). The functions $\zeta(q)$ were estimated from the linear behavior of the temperature and fluorescence structure functions, $\langle(\Delta T(\tau))^q\rangle$ and $\langle(\Delta F(\tau))^q\rangle$, as a function of the time scale τ in a log–log plot for values of q ranging from 0.1 to 5 with 0.05 increments.

The clear non-linearity of the functions $\zeta(q)$ illustrates the multifractal (i.e. patchy) character of small-scale temperature and phytoplankton distributions. It confirms and generalizes in different hydrodynamic and tidal regimes the multifractal nature of temperature and fluorescence previously demonstrated elsewhere using a global and local approaches (Seuront et al., 1996a, 1999, 2002; Seuront, 2004). More specifically, the scaling of

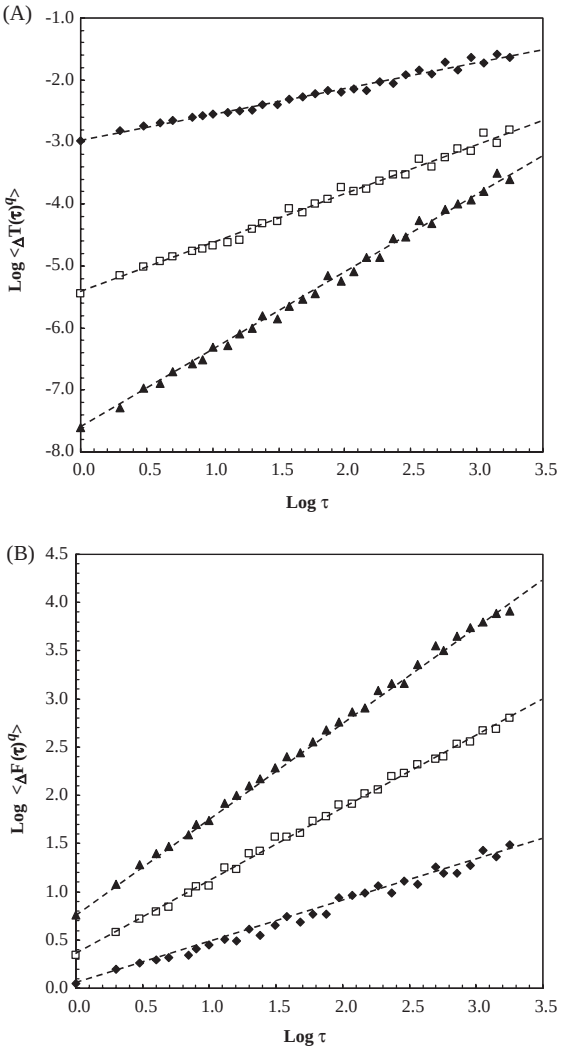

Fig. 3. The structure functions $\langle\Delta T(\tau)^q\rangle$ and $\langle\Delta F(\tau)^q\rangle$ versus the time scale τ in log–log plots for temperature (A) and in vivo fluorescence (B) simultaneously recorded during flood tide, shown for the orders of moment $q = 1$ (black diamonds), $q = 2$ (open squares) and $q = 3$ (black triangles).

the first moments $\zeta(1) = H$ leads to a behavior very similar to the one observed in the case of the spectral exponents β; an analysis of covariance thus did not identify any significant differences within each set of temperature and fluorescence subseries ($p > 0.05$), nor between the six sets considered ($p > 0.05$). The mean fluctuations of phytoplankton biomass can then be regarded as

being fully similar to those of a purely passive scalar.

However, while the functions $\zeta(q)$ estimated for temperature time series remain the same across variable turbulence and tidal conditions, the nonlinearity (i.e. convexity) of the functions $\zeta(q)$ estimated for fluorescence time series is lower during flood tide than during ebb tide for a given turbulence level, and clearly increases when the value of the dissipation rate ε decreases in flood and ebb tide conditions (Fig. 4). In addition, an analysis of covariance demonstrates that the functions $\zeta_{FT}(q)$ and $\zeta_{ET}(q)$ estimated from fluorescence time series in similar turbulent conditions in flood and ebb tide conditions are significantly different ($p<0.05$) for values of the statistical order of moment $q\geqslant 2.5$. Flood and ebb tide phytoplankton populations can nevertheless exhibit very similar levels of patchiness for the highest and lowest turbulent conditions considered in flood and ebb tides, i.e. 10^{-5}, 5×10^{-5} and $10^{-4}\,m^2\,s^{-3}$ (Fig. 4). Finally, phytoplankton distributions are respectively more and less patchy than a purely passive scalar in flood and ebb tide conditions.

More specifically, in flood tide, the functions $\zeta_{FT}(q)$ and $\zeta_T(q)$ cannot be distinguished for turbulence intensity of $10^{-6}\,m^2\,s^{-3}$. For lower and higher turbulence intensities, they diverge significantly for orders of moment $q\geqslant 3.00$. Alternatively, during ebb tide, the functions $\zeta_{ET}(q)$ and $\zeta_T(q)$ are never significantly different for $\varepsilon=10^{-5}\,m^2\,s^{-3}$, but start to diverge significantly for orders of moment $q\geqslant 3.25$ and $\geqslant 4.50$ for turbulence intensities $\varepsilon=10^{-4}$, 5×10^{-6}, 10^{-6} and $5\times10^{-7}\,m^2\,s^{-3}$, and $5\times10^{-5}\,m^2\,s^{-3}$, respectively.

In other words, the gradients observed in phytoplankton concentrations are higher than temperature in flood conditions, whatever the intensity of turbulence. Conversely, ebb-tide phytoplankton populations exhibit weaker gradients than temperature, and can then be considered as more homogeneously distributed than a passive scalar. The distribution of temperature then remains the same whatever the hydrodynamic and tidal conditions. This result is fully congruent with previous observations regarding the distribution of turbulent velocity fields (Seuront et al., 2005; Seuront and Schmitt, 2005) and passive scalars (Seuront, 2004), and confirms the passive scalar behavior of temperature. In contrast, for a given intensity of turbulence the distribution of

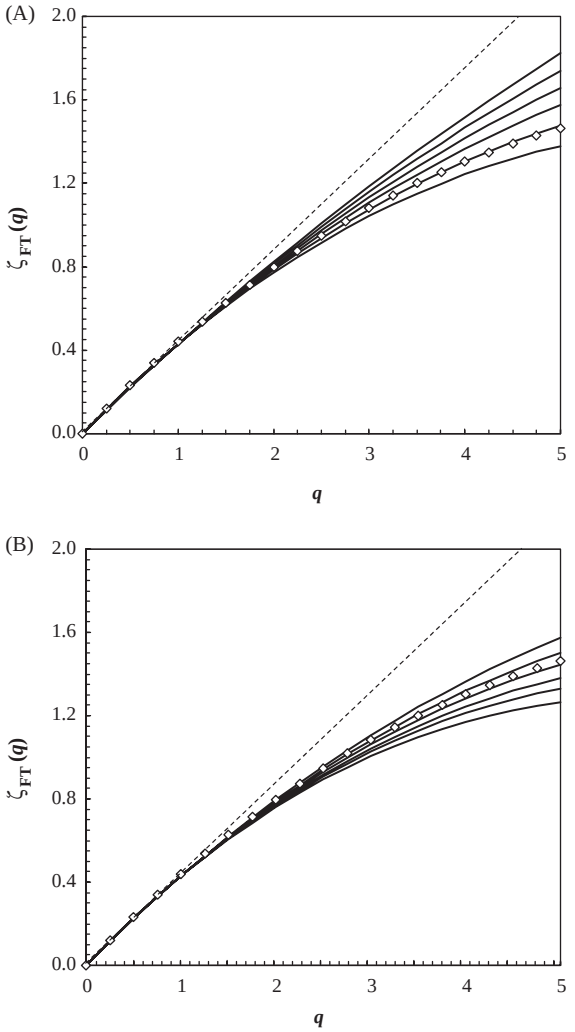

Fig. 4. The empirical scaling function $\zeta(q)$ estimated for in vivo fluorescence during flood tide (A) and ebb tide (B), compared to the empirical exponents estimated for temperature (open diamonds) and the theoretical homogeneous linear case $\zeta(q)=qH$ (dashed line). It is clear from the nonlinearity of $\zeta(q)$ that phytoplankton distributions are far from homogeneously distributed and in both tidal conditions patchiness increase with decreasing values of the turbulent energy dissipation rates. The energy dissipation rates considered here are from bottom to top are: 5.07×10^{-7}, 1×10^{-6}, 5×10^{-6}, 1×10^{-5}, 5×10^{-5}, and $1\times10^{-4}\,m^2\,s^{-3}$.

phytoplankton biomass is more and less intermittent than temperature in flood- and ebb-tide conditions, respectively (Fig. 4). In both tidal conditions, phytoplankton cells are more homogeneously distributed under high-turbulence conditions. This suggests that phytoplankton cells behave more like a passive scalar in low-turbulence conditions during flood tide (Fig. 4A) and in high-turbulence conditions during ebb tide (Fig. 4B). Alternatively, phytoplankton cells exhibit very specific properties (i.e. a more homogeneous, less intermittent behavior) under higher-turbulence conditions during flood tide and under lower-turbulence conditions of turbulence during ebb tide.

3.3. Turbulence and biophysical couplings

In Fig. 5 we present spectra of squared-coherence for the 24-pair combinations of temperature and fluorescence time series simultaneously sampled during flood tide for scales ranging between lower and higher limits of the scaling range previously estimated from power spectral and structure functions analyses (Figs. 2 and 3). The squared-coherence is clearly smaller than the 95% significance level, estimated from uncorrelated series presenting the same spectral characteristic than our empirical time series. Similar results have been obtained for temperature and fluorescence time series sampled during ebb tide, suggesting a statistical independence between the mean fluctuations of temperature and phytoplankton whatever the hydrodynamic and tidal conditions.

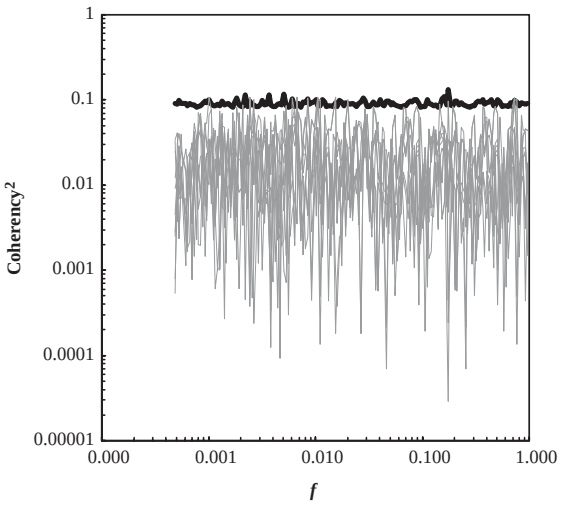

Fig. 5. Squared-coherence estimates for the 24-pair combinations of temperature and in vivo fluorescence time series simultaneously sampled during flood tide (gray lines) for scales ranging between lower and higher limits of the scaling range previously estimated from power spectral and structure functions analyses (see Figs. 3 and 4). The 95% significance levels (black line) are taken from 1000 coherence calculations between pairs of synthetic random uncorrelated data sets with the same spectral slope than the empirical ones.

In order to investigate further the nature of the dependence between temperature and phytoplankton distributions, we computed the Generalized Correlation Functions, $c(p,q)$ and the related Generalized Correlation Exponents, $r(p,q)$, between temperature and fluorescence time series, within each subset defined above. Fig. 6 shows the GCF, $c(p,q)$, plotted in log–log plots versus the time scale τ, for simultaneously recorded temperature and fluorescence time series in ebb tide (Fig. 6A) and in flood tide (Fig. 6B), as well as for temperature and fluorescence time series taken at different moments of the tidal cycle, and a fortiori independent (Fig. 7). The values of the functions $c(p,q)$ are higher during ebb tide (Fig. 6A) than during flood tide (Fig. 6B), suggesting a differential correlation between temperature and phytoplankton biomass fluctuations controlled by tidal processes. On the other hand, the weak values taken by the functions $c(p,q)$ estimated between independent temperature and fluorescence time series (Fig. 7) indicate a low correlation between temperature and phytoplankton biomass fluctuations. This is confirmed by the related values of the functions $r(p,q)$, which remain close to zero, whatever the combinations of p and q values (Fig. 8).

We subsequently refined these observations, comparing the functions $r(p,q)$ obtained between temperature and fluorescence time series in different tidal and turbulent conditions. Figs. 9 and 10 shows the functions $r(p,q)$ obtained for all combinations of p and q values with 0.1 increments for three levels of turbulence (10^{-4}, 10^{-5} and $10^{-6}\,m^2\,s^{-3}$) during ebb and flood tide, respectively. In both case, the correlation between

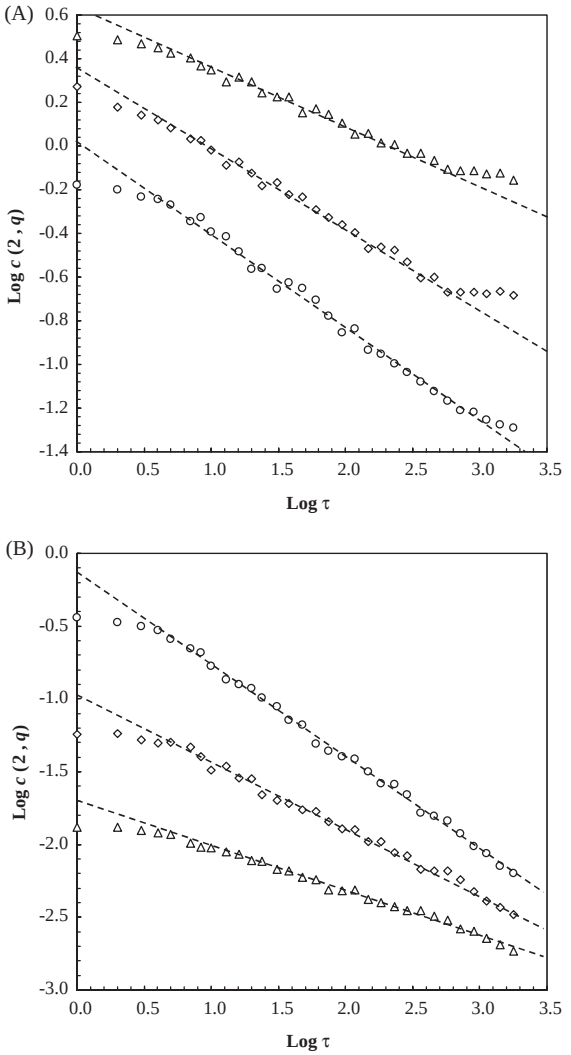

Fig. 6. The Generalized Correlation Function (GCF) $c(p,q)$ versus the time scale τ in log–log plots, for temperature and fluorescence time series simultaneously recorded during ebb tide (A) and flood tide (B). The function $c(p,q)$ shown here have been estimated for a constant value of the statistical order of moment p of temperature fluctuations ($p = 2$), and various values of the statistical order of moment q of in vivo fluorescence (i.e. $q = 1$, 2 and 3, from bottom to top). The slopes of the linear regression estimated over the scaling ranges (dashed lines) provide estimates of the Generalized Correlation Exponents (GCE) $r(p,q)$.

temperature and fluorescence fluctuations increases with increasing hydrodynamic conditions (Figs. 9A,B and Figs. 10A,B) and is weaker, even

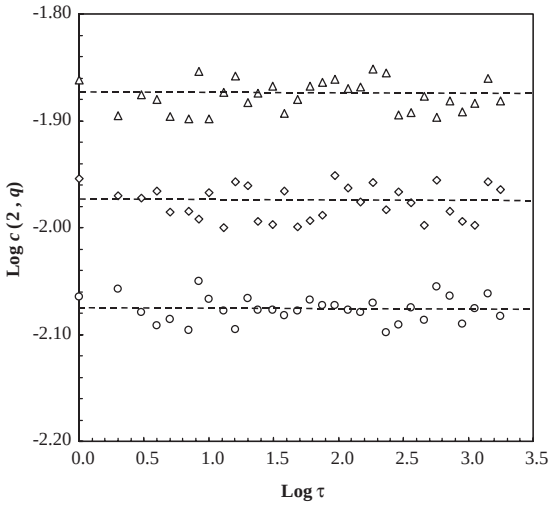

Fig. 7. The Generalized Correlation Function (GCF) $c(p,q)$ versus the time scale τ in log–log plots, for temperature and fluorescence time series recorded at different moments of the tidal cycle, and a fortiori independent. The function $c(p,q)$ shown here have been estimated for a constant value of the statistical order of moment p of temperature fluctuations ($p = 2$), and various values of the statistical order of moment p of in vivo fluorescence (i.e. $q = 1$, 2 and 3, from bottom to top). The slopes of the linear regression estimated over the scaling ranges (dashed lines) provide estimates of the Generalized Correlation Exponents (GCE) $r(p,q)$.

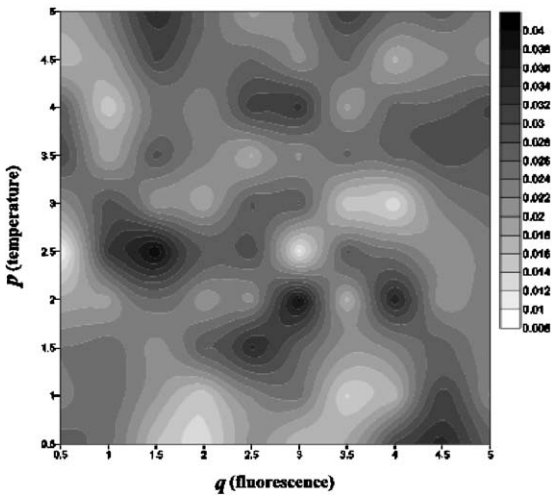

Fig. 8. The Generalized Correlation Exponents (GCE) $r(p,q)$ estimated for temperature and fluorescence time series recorded at different moment of the tidal cycle (and a fortiori independent), shown as a function of both p and q, which characterize temperature and in vivo fluorescence fluctuations, respectively.

nil, in low turbulent conditions (Figs. 9C and 10C). On the other hand, the decorrelation observed between temperature and phytoplankton fluctuations during both ebb and flood tide under weak turbulent conditions suggests an increase in the biological contributions to the control of phytoplankton biomass distribution, and confirms previous observations (cf. Fig. 4). Phytoplankton fluctuations then appear independent from the temperature fluctuations under the lowest turbulence levels investigated here, i.e. $5\times10^{-7}\,m^2\,s^{-3}$ (Figs. 9C and 10C). We thus confirm here the differential physical control suggested under strong turbulent conditions from the analysis of the shape of the function $\zeta_F(q)$, and its comparison with the function $\zeta_T(q)$; see Fig. 4.

More specifically, while the patterns of $r(p,q)$ during ebb tide (Figs. 9A and B) are more complex than those observed during flood tide (Figs. 10A and B), the overall shape of the functions $r(p,q)$ indicates that large phytoplankton fluctuations are associated—under sufficiently turbulent conditions—to strong temperature gradients, and conversely. This tendency seems to reflect, over a slightly wider range of scales, findings of Desiderio et al. (1993) who observed the occurrence of 0.1–0.2 m thick fluorescent layers just above local temperature gradients. These qualitative comments suggest a proportionality relationship between temperature and phytoplankton fluctuations. In case of perfect proportionality $\Delta F_\tau = K\Delta T_\tau$, where K is a constant, or for "random proportionality" $\Delta F_\tau = \kappa\Delta T_\tau$, where κ is a random variable independent on y, the function $r(p,q)$ should verify the relation (Seuront and Schmitt, 2005):

$$r(p,q) = \zeta_Y(p) + \zeta_Y(q) - \zeta_Y(p+q). \tag{11}$$

Relation (11) has nevertheless never been verified here. The phytoplankton fluctuations then cannot be regarded as being strictly proportional, nor randomly proportional to the fluctuations of temperature, i.e. $\Delta F = K.\Delta T$ and $\Delta F = \kappa.\Delta T$, respectively. On the other hand, the relation expected in case of $\Delta F_\tau \propto (\Delta T_\tau)^b$ writes (Seuront and Schmitt, 2005):

$$r(p,q) = \zeta_Y(bp) + \zeta_Y(q) - \zeta_Y(bp+q) \tag{12}$$

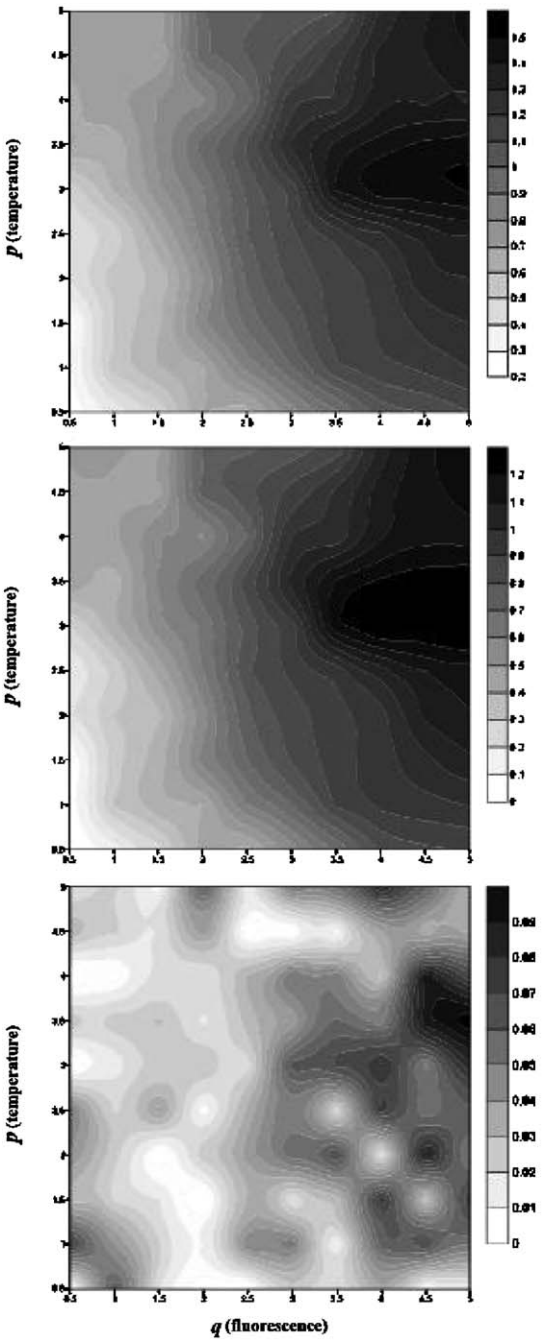

Fig. 9. The Generalized Correlation Exponents (GCE) $r(p,q)$, shown as a function of both p and q, which characterize temperature and in vivo fluorescence fluctuations, respectively. The functions $r(p,q)$ correspond to three different levels of turbulence, i.e. $\varepsilon = 10^{-4}$ (A), 10^{-5} (B) and $10^{-6}\,m^2\,s^{-3}$ (C) investigated during ebb tide.

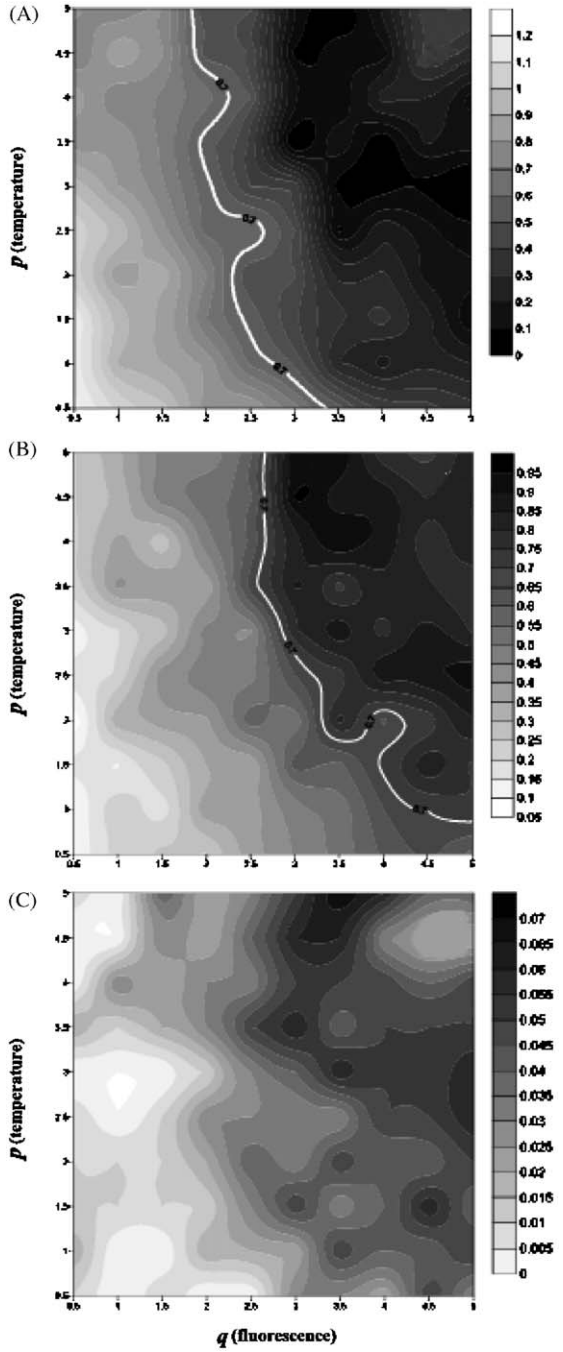

Fig. 10. The Generalized Correlation Exponents (GCE) $r(p,q)$, shown as a function of both p and q, which characterize temperature and in vivo fluorescence fluctuations, respectively. The functions $r(p,q)$ correspond to three different levels of turbulence, i.e. $\varepsilon = 10^{-4}$ (A), 10^{-5} (B) and $10^{-6}\,m^2\,s^{-3}$ (C) investigated during flood tide.

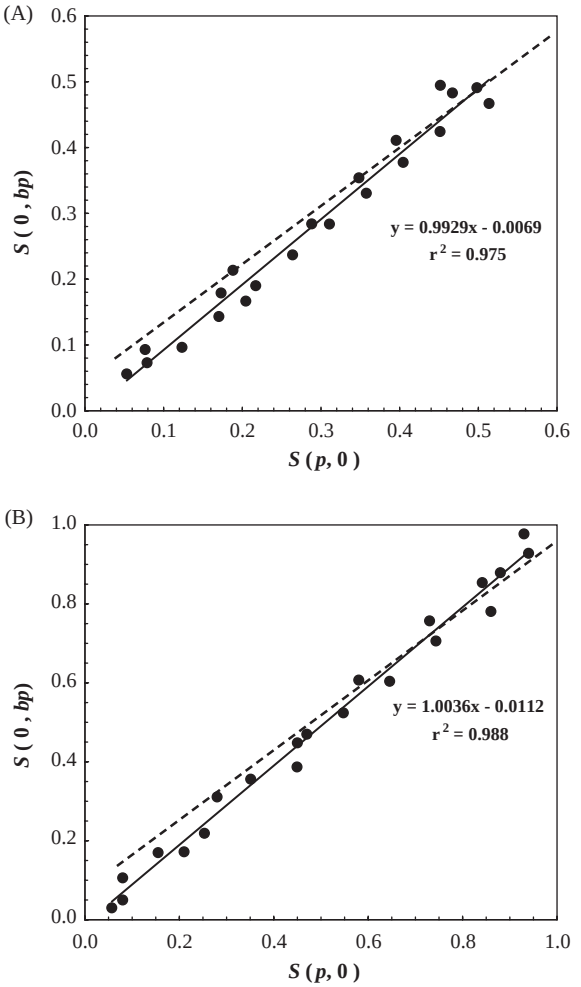

Fig. 11. Plots of the Generalized Correlation Exponents $S(p,0)$ versus $S(0,bp)$ for two levels of turbulence, $\varepsilon = 10^{-4}$ with $b = 0.90$ (A) and $\varepsilon = 10^{-5}$ with $b = 0.80$ (B). The slopes of the regression lines (continuous line) cannot be distinguished from the one of the relation $bp = q$ (dashed line). This shows the validity of Eq. (12), and the symmetry of the functions $r(p,q)$ in the bp–q plane.

and the value of b is estimated as the positive value such that (Seuront and Schmitt, 2005):

$$S(p,0) = S(0,bp). \tag{13}$$

"Eq. (12) has been verified testing the validity of Eq. (13) over a wide range of b values. Using b values ranging between 0.05 and 2 (with 0.05 increments), we then showed that Eq. (12) is verified for four of the six levels of turbulence

levels investigated during ebb tide, i.e. $\varepsilon = 10^{-4}\,m^2 \cdot s^{-3}$ with $b = 0.90$, $\varepsilon = 5.10^{-5}\,m^2 \cdot s^{-3}$ with $b = 0.85$, $\varepsilon = 10^{-5}\,m^2 \cdot s^{-3}$ with $b = 0.80$ and $\varepsilon = 5 \times 10^{-6}\,m^2 \cdot s^{-3}$ with $b = 0.78$, and two of the six turbulence levels investigated during flood tide, i.e. $\varepsilon = 10^{-4}\,m^2 \cdot s^{-3}$ with $b = 0.96$ and $\varepsilon = 5.10^{-5}\,m^2 \cdot s^{-3}$ with $b = 0.91$. Fig. 11 shows the relation $S(p,0)$ vs. $S(0,bp)$ corresponding to the functions $r(p,q)$ shown in Fig. 9a and b, with $b = 0.90$ and $b = 0.80$, respectively. The correlation shown between temperature and phytoplankton fluctuations under high turbulent conditions, is then related to a power-law dependence relationship, of the form $\Delta F_\tau \propto (\Delta T_\tau)^b$."

4. Discussion

4.1. Small-scale phytoplankton patchiness: inshore versus offshore waters

We stress that the above stated hypothesis of higher phytoplankton patchiness, based on fluorescence as a proxy of phytoplankton concentration, in coastal waters is supported by a set of converging arguments:

(i) Fluorescence, thus phytoplankton concentration, is significantly lower during our study period in offshore than inshore waters (Brylinski et al., 1991; Brunet et al., 1996; Breton et al., 2000; Seuront et al., 1999, 2002). Considering that more sparsely distributed algae are less likely to encounter and then to form aggregates (e.g., Jackson, 1990; Kiørboe, 2001), phytoplankton patchiness can be expected to be lower in offshore waters. This is consistent with previous observations conducted in the same area (Seuront, 1999; Seuront and Lagadeuc, 1998).

(ii) Green algae, Chrysophyceae and nanoplankton are more abundant in the coastal waters during the spring phytoplankton bloom (Breton, 2000). Most of these algae being motile, they are likely to exhibit some behavioral response to physical gradients such as nutrient point source previously observed in the same area (Seuront et al., 2002). They can then be expected to produce local aggregates via chemotaxis (e.g., Childress et al., 1975; Kessler, 1985, 1986). Gyrotaxis, as a result of the interaction between cell morphology and motility with local shear, is another example of a community response to the abiotic template likely to produce coherent spatial structure of phytoplankton cells (Kessler, 1985; Mitchell et al., 1990). The basic assumption is that gyrotactic clustering occurs only in high cell concentrations (i.e. 10^3–10^7 cell cm^{-3}; Kessler, 1985) where there is sufficient biological activity to generate local shear. As cell counts realized in the inshore waters of the Eastern English Channel during our sampling period (Breton, 2000; Seuront and Souissi, 2002) are fully compatible with the above-stated concentrations, gyrotaxis may potentially be responsible for a higher phytoplankton patchiness in the inshore than in the offshore waters.

(iii) During the sampling experiment, the Prymnesiophyceae *Phaeocystis* sp., known to dominate the phytoplankton community of the coastal waters of the Eastern English Channel during spring blooms (Seuront et al., 2002), reached high concentrations during the sampling experiment (Seuront and Souissi, 2002). The genus *Phaeocystis*, known for its highly developed swarming capacities (Seuront et al., 2002; Verity and Medlin, 2003), it is likely to be responsible for a higher patchiness in coastal waters.

4.2. Small-scale phytoplankton patchiness and tidal conditions

Considering the above-stated congruent arguments, it is likely that phytoplankton biomass is more patchily distributed inshore than offshore in the Eastern English Channel. As the intensities of all the fluorescence time series analyzed here were not significantly different, the observed decrease in phytoplankton patchiness during flood tide then could not be related to any 'density-dependent effect' but instead to a 'population-dependent effect'. The offshore waters are advected towards the coast during flood tide. The more homogeneous offshore phytoplankton population then decrease the patchiness of the phytoplankton populations observed from our sampling station. Alternatively, the inshore patchy population are advected offshore during ebb tide and subsequently increase the observed level of patchiness.

4.3. Small-scale phytoplankton patchiness and hydrodynamic conditions

The effects of the semidiurnal tidal cycle (high–low tide) on phytoplankton distribution were studied from fluorescence time series recorded from a single depth (5 m). The relevance of our results as being representative of the phytoplankton patchiness conditions actually experienced over the entire water column can be ensured only by the absence of any differential vertical distribution of phytoplankton biomass in the water column. As our sampling experiment was conducted in a period of spring tide, no physical vertical stratification of the water column is likely to occur (Brylinski et al., 1984, 1991, 1996; Lagadeuc et al., 1997). The absence of a vertical gradient of density, as well as the high dissipation rates and the low dynamic stability, indicate that the water column was always highly mixed. In these conditions, surface accumulation of ultraplankton due to a low sinking rate of small cells (Raimbault et al., 1989), or flagellates due to an active displacement in the upper layer (Kamykowski et al., 1997), as well as fast sinking of senescent *Phaeocystis* colonies (Andreassen and Wassman, 1998; Peperzak et al., 2003), are unlikely to occur.

Theoretical analyses of particles coagulation processes predict that aggregate formation depends on the probability of particle collision and the efficiency with which two colliding particles then coagulate (Jackson, 1990; Kiørboe et al., 1994). The former is a function of particle concentration, size and the mechanism by which particles are brought into contact, e.g., Brownian motion, shear or the differential settlement of particles. The latter mainly depends on the physico-chemical properties of the particle surface and may vary with the particle type. As encounter rates increase with increasing turbulence intensity, the size of the aggregate, and thus the level of patchiness would be expected to increase with turbulence. We have, however, shown that phytoplankton patchiness decreases with increasing turbulence intensity, in flood tide and ebb tide (see Fig. 4) Turbulence cannot be thought as a direct driving process in the creation of phytoplankton patchiness over the range of turbulence intensities investigated here. It is likely, instead, that above a given threshold turbulent diffusion overcomes the effects of biological stickiness and leads to a decrease in aggregate size, and thus to a decrease in the observed patchiness. Our results also suggest differential stickiness efficiency of inshore and offshore phytoplankton populations. Offshore populations advected inshore during flood tide could be less sticky than inshore populations advected offshore during ebb tide, and thus less likely to maintain their cohesion with increasing turbulent diffusive processes. This hypothesis is consistent with the difference observed in phytoplankton species composition in offshore and inshore waters. For instance, inshore and offshore Prymnesiophyceae are respectively dominated by the genus *Phaeocystis* sp. (Seuront and Souissi, 2002; Seuront et al., 2002) and the species *Emiliana huxleyi* (Brylinski et al., 1991), the former being likely to be stickier.

4.4. Scaling independence versus multiscaling dependence

The results provided by squared-coherence analyses (Fig. 7) could have led us to conclude to the absence of significant coupling between temperature and fluorescence time series over the whole range of scales, tidal and turbulent conditions investigated. However, the Generalized Correlation Functions $c(p,q)$, as well as their related Generalized Correlation Exponents, $r(p,q)$, led to different conclusions.

First, the higher values of the functions $c(p,q)$ obtained between temperature and fluorescence time series sampled during ebb tide suggest (see Fig. 8) a stronger coupling between temperature and phytoplankton fluctuations during ebb tide. While further work is needed to provide a mechanistic explanation to the observed differential coupling, it is likely to be related to the differences between inshore and offshore waters in terms of species density and composition. Dense inshore phytoplankton populations with aggregative properties are, for instance, more likely to be more impacted by physical fluctuations than sparsely distributed offshore ones.

Second, while it has been shown that the multiscaling behavior of the functions $c(p,q)$ is coherent with the observations conducted using spectral and structure functions analyses, careful examinations of the correlation exponents $r(p,q)$ clearly show that the idea of statistical independence between the parameters investigated here should be abandoned, especially for high values of the statistical orders of moment p and q, i.e. $p>2$ and $q>2$ (Figs. 9 and 10). Namely, further investigation of the patterns exhibited by the correlation exponents $r(p,q)$ estimated between temperature and fluorescence showed that temperature and phytoplankton abundance fluctuations are related by a power-law dependence relationship, i.e. $\Delta F_\tau \propto (\Delta T_\tau)^b$, under high turbulent conditions and did not exhibit any significant relationship under low turbulent conditions. The observed power-law exponents b are significantly higher during ebb tide than during flood tide, suggesting a stronger biophysical coupling in the inshore than in the offshore waters. Even in the absence of any clear mechanism to explain the differential patterns observed, we stress that the present results are nevertheless consistent with both empirical and theoretical work, demonstrating that the intermittent character of turbulence is responsible for the creations of strong discontinuities (''ramps'') in the distribution of passive scalars: the strongest scalars discontinuities are related, and then coupled, to the strongest velocity discontinuities.

More generally, the results presented here then lead to replace the concept of statistical independence, which might have been considered using standard squared-coherence analysis, by the more accurate concept of differential statistical independence. Indeed, this independence obviously exists if one only deals with low orders of moment, and needs to be replaced by a more general high-order dependence.

4.5. Multiscaling, biophysical couplings and sampling techniques

Let us mention here that at this stage of the development of the multiscaling techniques illustrated in the present paper, the presence and the absence of evidence for power-law dependence between phytoplankton and temperature fluctuations cannot (a priori) be regarded as a general rule driving biophysical couplings in pelagic ecosystems. Indeed, the relationship between temperature and fluorescence, or more generally biophysical couplings, can be influenced, and then made more complex, by both the processes related to phytoplankton cells ecology and to the sampling strategy. Over the range of scales investigated in the present study, fluorescence fluctuations can indeed result from nonlinear interactions between the physiological state of phytoplankton cells, their related coagulation ability, the specific composition of phytoplankton assemblages, the grazing impact of copepods (shown recently to influence both spectral and multifractal properties of phytoplankton biomass; Seuront, 1999; Lovejoy et al., 2001), and the turbulent processes. The resulting fluctuations can then be potentially more complex than those observed for a purely passive scalar as temperature.

On the other hand, considering (i) the highly intrusive character of the sampling device used to record temperature and fluorescence (a Sea-Bird 25 Sealogger CTD probe and a Sea Tech fluorometer, respectively), and (ii) the spatial separation of the temperature and fluorescence sensors (≈ 10 cm), it is reasonable to think that the most extreme events, which are also the most rare and contribute to the highest values of the moments p and q, are not necessarily simultaneously sampled in a proper way, leading to spurious joint high-order properties. In particular, this could explain the weakening of the Generalized Correlation Exponents, $r(p,q)$, for values of the moments p and q such as $p \geqslant 4$ and $q \geqslant 4$. The latter limitation will be easily fixed in the near future considering the increasing development and availability of micro structure profilers able to record both physical and biological parameters with a high-spatial resolution from mildly intrusive sensors (Wolk et al., 2002, 2004). On the other hand, the intrusive character of the sampling devices will be difficult to overcome, because of the intrinsic physiological, biological and ecological processes affecting phytoplankton populations.

5. Conclusion: the cost and gain of increasing analysis complexity

Our results demonstrate that single scaling properties of temperature and phytoplankton would have erroneously let to conclude that the latter could be regarded as a purely passive scalar. However, investigations of their detailed variability in the multifractal framework lead to consider that phytoplankton distributions present very specific properties, depending on (i) the nature of tidal processes, and (ii) the intensity of local turbulent processes. This suggests a differential control of phytoplankton distribution involving complex interactions between turbulent velocity fields, and the involved particles properties such as buoyancy, size, density or aggregative properties. In particular, this assertion is supported by the specific behavior of phytoplankton multiscaling properties under low-turbulence conditions, suggesting the prevalence of phytoplankton cells specific properties on turbulent processes.

This has been confirmed and specified by the introduction of the Generalized Correlation Functions/Exponents. The correlation—and then the couplings—between temperature and phytoplankton biomass fluctuations are thus higher under high hydrodynamic forcing, and decrease progressively to collapse under low hydrodynamic forcing. In particular, careful examination of the functions $r(p,q)$ indicates that large phytoplankton fluctuations are associated—under strong enough turbulent conditions—to weak temperature gradients, and conversely. These results are consistent with more intuitive and qualitative results by Desiderio et al. (1993) over similar scales, and Wolk et al. (2002, 2004) at smaller scales. Even if additional work and data sets will be needed to achieve more definitive functional scenarios, the joint multifractal framework introduced here provides the first objective method to characterize, both qualitatively and quantitatively, the details of the relationships between any couple of simultaneously recorded patterns or processes. In particular, this framework makes no assumptions about the spectrum or the distribution of either data set, and it takes fully into account their intrinsic multiscaling properties.

Finally, regarding the additional quantity of informations brought by the univariate and bivariate multiscaling procedures described here to our understanding of the structure of velocity, temperature and phytoplankton fluctuations, as well as the couplings between temperature and phytoplankton biomass, we claimed, as already stressed elsewhere (e.g., Yamazaki, 1993; Seuront et al., 2001), that taking into account the reality of the intermittent nature of bio-physical microstructures could be the first step towards a general understanding of structures and functions in marine pelagic ecosystems. The quite elevated cost associated to making use of the single and joint multifractal tools presented here in terms of algorithmic developments and computation time consumption will then be easily overcome by the valuable gain in emerging knowledge.

Acknowledgments

We thank the organizers of the Warnemünde Turbulence Days 2003 for their kind invitation to contribute to this volume. We are grateful to Prof. H. Yamazaki and Prof. C. Garrett for their enthusiasm and support during the development of the '*Generalized Correlation Functions*' framework, and to the members of the Ocean Ecosystem Dynamics Laboratory (Department of Ocean Sciences, Tokyo University of Fisheries, Japan) for their enjoyable discussion and company. This work was originally supported by a postdoctoral fellowship from the Japan Society for the Promotion of Science and a Monbusho Grant-in-Aid for JSPS Fellows (No. 99756) to L. Seuront. Thanks are extended to the captain and crew of the NO 'Sepia II' for their help during the sampling experiment. We thank the anonymous referee for his constructive comments and criticisms from which this paper benefited greatly. This work is a contribution of the Ecosystem Complexity Research Group.

References

Andreassen, I.J., Wassman, P., 1998. Vertical flux of phytoplankton and particulate biogenic matter in the marginal ice

zone of the Barents Sea in May 1993. Marine Ecology Progress Series 170, 1–14.

Blackburn, N., Fenchel, T., Mitchell, J.G., 1998. Microscale nutrient patches in planktonic habitats shown by chemotactic bacteria. Science 282, 2254–2256.

Bowers, D.G., Simpson, J.H., 1987. Mean position of tidal fronts in European-shelf seas. Continental Shelf Research 7, 35–44.

Breton, E., 2000. Qualité du pool nutritif et nutrition des copépodes pélagiques en Manche orientale. Ph.D. Thesis, Université du Littoral Côte d'Opale, France.

Breton, E., Brunet, C., Sautour, B., Brylinski, J.M., 2000. Annual variations of phytoplankton biomass in the Eastern English Channel: comparison by pigments signatures and microscopic counts. Journal of Plankton Research 22, 1423–1440.

Brunet, C., Brylinski, J.M., Degros, N., Hilde, D., 1992. Productivity, photosynthetic pigments and hydrology in the coastal front of the Eastern English Channel. Journal of Plankton Research 14, 1541–1552.

Brunet, C., Brylinski, J.M., Lemoine, Y., 1993. In situ variations of the xanthophylls dioxanthin and diadinoxanthin: photoadaptation and relationships with a hydrodynamical system in the eastern English Channel. Marine Ecology Progress Series 102, 69–77.

Brunet, C., Brylinski, J.M., Bodineau, L., Thoumelin, G., Bentley, D., Hilde, D., 1996. Phytoplankton dynamics during the spring bloom in the south-Eastern English Channel. Estuarine Coastal and Shelf Science 43, 469–483.

Brylinski, J.M., Lagadeuc, Y., 1990. L'interface eau côtière/eau du large dans le Pad-de-Calais (côte française): une zone frontale. Comptes Rendus de l' Academie Sciences Paris Série II 311, 535–540.

Brylinski, J.M., Dupont, J., Bentley, D., 1984. Conditions hydrologiques au large du cap Griz-Nez (France): premiers résultats. Oceanologica Acta 7, 315–322.

Brylinski, J.M., Lagadeuc, Y., Gentilhomme, V., Dupont, J.P., Lafite, R., Dupeuple, P.A., Huault, M.F., Auger, Y., Puskaric, E., Wartel, M., Cabioch, L., 1991. Le "fleuve côtier": un phénomène hydrologique important en Manche orientale. Exemple du Pas-de-Calais. Oceanologica Acta 11, 197–203.

Brylinski, J.M., Brunet, C., Bentley, D., Thoumelin, G., Hilde, D., 1996. Hydrography and phytoplankton biomass in the Eastern English Channel in spring 1992. Estuarine Coastal and Shelf Science 43, 507–519.

Cassie, R.M., 1963. Microdistribution in the plankton. Oceanography and Marine Biology—An Annual Review 1, 223–252.

Childress, S., Levandowsky, M., Spiegel, E.A., 1975. Pattern formation in a suspension of swimming micro-organisms: equations and stability theory. Journal of Fluid Mechanics 63, 591–613.

Corrsin, S., 1951. On the spectrum of isotropic temperature in an isotropic turbulence. Journal of Applied Physics 22, 469.

Cowles, T.J., Desiderio, R.A., Neuer, W.S., 1993. In situ characterisation of phytoplankton from vertical profiles of fluorescence spectra. Marine Biology 115, 217–222.

Desiderio, R.A., Cowles, T.J., Moum, J.N., 1993. Microstructure profiles of laser-induced chlorophyll fluorescence spectra: evaluation of backscatter and forward-scatter fiber-optic sensors. Journal of Atmospheric and Oceanic Technology 10, 209–224.

Dupont, J.P., Lafite, R., Huault, M.F., Lamboy, M., Brylisnki, J.M., Guéguéniat, P., 1991. La dynamique des masses d'eau et matière en suspension en Manche orientale. Oceanologica Acta 11, 177–186.

Falkowski, P.G., Kiefer, D.A., 1985. Chlorophyll *a* fluorescence in phytoplankton: a comparative field study. Journal of Marine Research 7, 715–731.

Frisch, U., 1995. Turbulence. Cambridge University Press, Cambridge.

Furhman, J.A., 1999. Marine viruses and their biogeochemical and ecological effects. Nature 399, 541–548.

Gargett, A.E., 1997. "Theories" and techniques for observing turbulence in the euphotic zone. Scientia Marina 61, 25–45.

Gerritsen, J., Strickler, J.R., 1977. Encounter probablities and community structure in zooplankton: a mathematical model. Journal of the Fisheries Research Board of Canada 34, 73–82.

Itsweire, E.C., Osborn, T.R., Stanton, T.P., 1989. Horizontal distribution and characteristics of shear layers in the seasonal thermocline. Journal of Physical Oceanography 10, 301–320.

Jackson, G., 1990. A model for the formation of marine algal flocks by physical coagulation processes. Deep-Sea Research 37, 1197–1211.

Jaffe, J.S., Franks, P.J.S., Leising, A.W., 1998. Simultaneous imaging of phytoplankton and zooplankton distributions. Oceanography 11, 24–29.

Jiménez, J., 1997. Oceanic turbulence at millimeter scales. Scientia Marina 61, 47–56.

Jou, D., 1997. Intermittent turbulence: a short introduction. Scientia Marina 61, 57–62.

Kamykowski, D., Yamazaki, H., Yamazaki, A.K., Kirkpatrick, G., 1997. A comparison of how different orientation behaviours influence dinoflagellate trajectories and photoresponses in turbulent water columns. In: Anderson, D.M., Cambella, A.D., Hallegraeff, G.M. (Eds.), The Physical Ecology of Harmful Algal Blooms. Springer, Berlin, pp. 581–599.

Karp-Boss, L., Boss, E., Jumars, P., 1996. Nutrient fluxes to planktonic osmotrophs in the presence of fluid motion. Oceanography and Marine Biology—An Annual Review 34, 71–104.

Kessler, J., 1985. Hydrodynamic focussing of motile algal cells. Nature 313, 218–220.

Kessler, J., 1986. Individual and collective dynamics of swimming cells. Journal of Fluid Mechanics 173, 191–205.

Kiørboe, T., 2001. Formation and the fate of marine snow: small-scale processes with large scale implications. Scientia Marina 65, 57–71.

Kiørboe, T., Lunsgaard, C., Olesen, M., Hansen, J.L.S., 1994. Aggregation and sedimentation processes during a spring

phytoplankton bloom: a field experiment to test coagulation theory. Journal of Marine Research 52, 297–323.

Kirk, J.T.O., 1994. Light and Photosynthesis in Aquatic Systems. Cambridge University Press, Cambridge.

Kolmogorov, A.N., 1941. The local structure of turbulence in incompressible viscous fluid for very large Reynolds numbers. Doklady Akademii Nauk SSSR 30, 299–303.

Lagadeuc, Y., Brylinski, J.M., Aelbrecht, D., 1997. Temporal variability of the vertical stratification of a front in a tidal Region of Freshwater Influence (ROFI) system. Journal of Marine Research 12, 147–155.

Legendre, P., Legendre, L., 1998. Numerical Ecology. Elsevier, Amsterdam.

Lovejoy, S., Currie, W.J.S., Tessier, Y., Claereboudt, M.R., Bourget, E., Roff, J.C., Schertzer, D., 2001. Universal multifractals and ocean patchiness: phytoplankton, physical fields and coastal heterogeneity. Journal of Plankton Research 23, 117–141.

MacKenzie, B.R., Leggett, W.C., 1991. Quantifying the contribution of small-scale turbulence to the encounter rates between larval fish and their zooplankton prey: effects of wind and tide. Marine Ecology Progress Series 73, 149–160.

MacKenzie, B.R., Leggett, W.C., 1993. Wind-based models for estimating the dissipation rates of turbulence energy in aquatic environments: empirical comparisons. Marine Ecology Progress Series 94, 207–216.

Mann, K.H., Lazier, J.R.N., 1996. Dynamics of Marine Ecosystems. Blackwell, Boston.

Marrasé, C., Saiz, E., Redondo, J.M., 1997. Lectures on plankton and turbulence. Scientia Marina 61, 7–228.

Martin-Jezequel, V., 1983. Fracteurs hydrologiques et phytoplankton en Baie de Morlaix (Manche occidentale). Hydrobiologia 102, 131–143.

McAlice, B.J., 1970. Observations on the small-scale distribution of estuarine phytoplankton. Marine Biology 7, 100–111.

Mitchell, J.G., Fuhrman, J.A., 1989. Centimeter scale vertical heterogeneity in bacteria and chlorophyll *a*. Marine Ecology Progress Series 54, 141–148.

Mitchell, J.G., Okubo, A., Fuhrman, J.A., 1990. Gyrotaxis as a new mechanism for generating spatial heterogeneity and migration in microplankton. Limnology and Oceanography 35, 123–130.

Obukhov, A.M., 1941. Spectral energy distribution in a turbulent flow. Doklady Akademii Nauk SSSR 32, 22–24.

Obukhov, A.M., 1949. Structure of the temperature field in a turbulent flow. Izvestiya Akademii Nauk SSSR Geographia I Jeofizik 13, 55.

Owen, R.W., 1989. Microscale and finescale variations of small plankton in coastal and pelagic environments. Journal of Marine Research 47, 197–240.

Peperzak, L., Colinj, F., Koeman, R., Gieskes, W.W.C., Joordens, J.C.A., 2003. Phytoplankton sinking rates in the Rhine region of freshwater influence. Journal of Plankton Research 25, 365–383.

Peters, F., Marrasé, C., 2000. Effects of turbulence on plankton: an overview of experimental evidence and some theoretical considerations. Marine Ecology Progress Series 205, 291–306.

Press, W.H., Teukolsky, S.A., Vetterling, W.T., Flannery, B.P., 1992. Numerical Recipes in Fortran 77. Cambridge University Press, Cambridge.

Raimbault, P., Taupier-Lepage, I., Rodier, M., 1989. Vertical size distribution of phytoplankton in the western Mediterranean Sea during early summer. Marine Ecology Progress Series 45, 153–158.

Sanford, L.P., 1997. Turbulent mixing in experimental ecosystem studies. Marine Ecology Progress Series 161, 265–293.

Seuront, L., 1999. Space–time heterogeneity and bio-physical coupling in pelagic ecologie: implications on carbon fluxes estimates. Ph.D. Thesis, University of Sciences and Technologies of Lille, France.

Seuront, L., 2004. Small-scale turbulence in the plankton: low-order deterministic chaos or high-order stochasticity? Physica A 341, 495–525.

Seuront, L., Lagadeuc, Y., 1998. Spatio-temporal structure of tidally mixed coastal waters: variability and heterogeneity. Journal of Plankton Research 20, 1387–1401.

Seuront, L., Schmitt, F.G., 2005. Multiscaling statistical procedures for the exploration of biophysical couplings in intermittent turbulence. Part II. Theory. Deep-Sea Research II, this issue [doi:10.1016/j.dsr2.2005.01.005].

Seuront, L., Souissi, S., 2002. Evidence for climatic control of *Phaeocystis* sp. bloom in the Eastern English Channel. La Mer 40, 41–51.

Seuront, L., Schmitt, F., Schertzer, D., Lagadeuc, Y., Lovejoy, S., 1996a. Multifractal intermittency of Eulerian and Lagrangian turbulence of ocean temperature and plankton fields. Nonlinear Processes in Geophysics 3, 236–246.

Seuront, L., Schmitt, F., Lagadeuc, Y., Schertzer, D., Lovejoy, S., Frontier, S., 1996b. Multifractal analysis of phytoplankton biomass and temperature in the ocean. Geophysical Research Letters 23, 3591–3594.

Seuront, L., Schmitt, F., Lagadeuc, Y., Schertzer, D., Lovejoy, S., 1999. Universal multifractal analysis as a tool to characterize multiscale intermittent patterns: example of phytoplankton distribution in turbulent coastal waters. Journal of Plankton Research 21, 877–922.

Seuront, L., Gentilhomme, V., Lagadeuc, Y., 2002. Small-scale nutrient patches in tidally mixed coastal waters. Marine Ecology Progress Series 232, 29–44.

Seuront, L., Yamazaki, H., Schmitt, F.G., 2005. Intermittency. In: Baumert, H., Sündermann, J., Simpson, J. (Eds.), Marine Turbulences: Theories, Observations and Models. 66–78.

Smayda, T.J., 2002. Turbulence, watermass stratification and harmful algal bloom: an alternative view and frontal zones as "pelagic seed bank". Harmful Algae 1, 95–102.

Strickland, J.D.H., Parsons, T.R., 1972. A practical handbook of seawater analysis. Bulletin of the Fisheries Research Board of Canada 167, 1–311.

Tomczak, M., Godfrey, J.S., 1994. Regional Oceanography: An Introduction. Pergamon, New York.

Verity, P.G., Medlin, L.K., 2003. Observations on colony formation by the cosmopolitan phytoplankton genus *Phaeocystis*. Journal of Marine Systems 43, 153–164.

Visser, A.W., 1997. Using random walks models to simulate the vertical distribution of particles in a turbulent water column. Marine Ecology Progress Series 158, 275–281.

Waters, R.L., Mitchell, J.G., 2002. Centimeter-scale spatial structure of estuarine in vivo fluorescence profiles. Marine Ecology Progress Series 237, 51–63.

Waters, R.L., Mitchell, J.G., Seymour, J.R., 2003. Geostatistical characterization of centimetre-scale spatial structure of in vivo fluorescence. Marine Ecology Progress Series 251, 49–58.

Wolk, F., Yamazaki, H., Seuront, L., Lueck, R.G., 2002. A new free-fall profiler for measuring biophysical microstructure. Journal of Atmospheric and Oceanic Technology 19, 780–793.

Wolk, F., Seuront, L., Yamazaki, H., Leterme, S., 2004. Comparison of biological scale resolution from CTD and microstructure measurements. In: Seuront, L., Strutton, P.G. (Eds.), Handbook of Scaling Methods in Aquatic Ecology. Measurement, Analysis, Simulation. CRC Press, Boca Raton, FL, pp. 3–16.

Yamazaki, H., 1993. Lagrangian study of planktonic organisms: perspectives. Bulletin of Marine Science 53, 265–278.

Yamazaki, H., Okubo, A., 1995. A simulation of grouping: an aggregative random walk. Ecological Modeling 79, 159–165.

Yin, K., Harrison, P.J., 2000. Influences of flood and ebb tides on nutrient fluxes and chlorophyll on an intertidal flat. Marine Ecology Progress Series 196, 75–85.